



Two-step synthesis of niobium doped Na–Ca–(Mg)–P–Si–O glasses

N. A. Wójcik^{1,2,*} , S. Ali², A. Mielewczyk-Gryń¹, and B. Jonson²

¹ Faculty of Applied Physics and Mathematics, Institute of Nanotechnology and Materials Engineering, Gdańsk University of Technology, Narutowicza Street 11/12, 80–233 Gdańsk, Poland

² Department of Built Environment and Energy Technology, Linnaeus University, 35195 Växjö, Sweden

Received: 12 October 2020

Accepted: 4 January 2021

Published online:
25 January 2021

© The Author(s) 2021

ABSTRACT

Niobium doped biosolubility glasses in the Na–Ca–(Mg)–P–Si–O system were prepared by using an untypical two-step synthesis route. The parent glass was melted in air atmosphere at 1350 °C followed by re-melting the glass in Nb crucible with the addition of metallic Mg/Ca powder in the nitrogen atmosphere. The second melting step was carried out at 1450–1650 °C, using an induction furnace. The topography and structure of the obtained glasses were characterized by confocal microscopy, X-ray powder diffraction and infrared spectroscopic techniques. The chemical compositions were examined by energy-dispersive X-ray spectroscopy (EDS). The glasses were found to be of grayish color, X-ray amorphous and having network connectivity between ~ 2.5 and 2.7 . The network connectivity of re-melted glasses was lower than the one of the parent glass. The glass structure consists of a highly disrupted silicate network of predominantly Q^2 groups as well as isolated orthophosphate tetrahedra. The parent glass contains nanocrystallites consisted of apatitic PO_4^{3-} groups. The re-melted glasses contain non-apatitic or amorphous calcium phosphates. The obtained glass transition temperatures range from 530 to 568 °C and exhibit higher values for glassed doped with Ca metal. These glasses have improved thermal stability as compared to reference bioglasses. The biosolubility test in phosphate buffered saline solution (PBS) confirms that the glasses have biosolubility properties and HAp formation on the surfaces was observed.

Introduction

Bioactive glasses are promising materials for the stimulation of bone regeneration; however, they have not yet reached their full potential [1]. Most studies

focused on relatively few silica-based compositions, such as 45S5 (46SiO₂–26.91CaO–24.35Na₂O–2.60P₂O₅ in mol%) and S53P4 (53.85SiO₂–21.77CaO–22.66Na₂O–1.72P₂O₅ mol%)[1–3] prepared in air, using the conventional melting technique. However, alternative methods for the preparation of bioactive

Handling Editor: David Cann

Address correspondence to E-mail: natalia.wojcik@pg.edu.pl

<https://doi.org/10.1007/s10853-021-05781-w>

glasses are also in the great interest, like sol-gel technique [1] and using a reducing atmosphere [4, 5]. In the current paper, a two-step synthesis route (described in [5]) with the addition of Mg/Ca metal and reducing atmosphere is applied, to prepare the potentially bioactive phospho-silicate glasses. This specific preparation technique allows to achieve glasses with unique structure and improved thermal properties due to incorporation of nitrogen into their network (e.g., through the addition of Si_3N_4) [6–9]. So far it was successfully applied to the preparation of bioactive oxynitride phosphate and [5] oxynitride silicate glasses [4, 10]. However, the bioactive oxynitride silicate glasses prepared by similar technique did not contain phosphorous, which significantly increase the bioactive properties of glass [11, 12] while nitrogen was found to have the opposite effect [4, 10].

One disadvantage of the well-known bioactive glasses 45S5 and S53P4 is their high tendency toward crystallization [13, 14]. These amorphous materials show a relatively high glass transition temperature; 45S5, $T_g = 552$ °C and S53P4, $T_g = 561$ °C [13]; however, their thermal stability is rather low; 163 °C for 45S5 and 187 °C for S53P4 [13, 14]. The thermal properties can be improved by compositional modifications. It has been shown that magnesium acts to aid the sintering window or “working range” and suppress crystallization, both very beneficial properties with respect to bioactivity [15, 16]. The niobium (Nb) is a relatively unexplored metallic ion in tissue engineering but it may have relevance for bone regenerative applications. It has been reported that Nb has a lower cytotoxicity than other metal ions [17] and has been shown to stimulate mineralization in human osteoblast populations [18, 19]. Moreover, the newest studies of Nb-containing 45S5 bioactive glasses (up to 1 mol% of Nb_2O_5) characterized them as having angiogenic potential [20]. In our previous paper [5], we have shown that phosphate glasses can dissolve Nb from the crucible material during melting while no Nb was found in silicate glasses [7, 8].

In the current paper, the first time a two-step preparation method with the addition of Mg/Ca metal and reducing atmosphere is applied, to prepare bioactive niobium doped phospho-silicate glasses containing significantly higher amounts of P_2O_5 than the widely studied reference bio glasses. Furthermore, the relationship between structure and thermal

properties is evaluated and the effect of Nb addition on biosolubility is discussed.

Materials and methods

Synthesis

Two series of silicate-based glasses doped with metallic Mg or Ca were prepared. First, the target glass $25\text{Na}_2\text{O}-20\text{CaO}-5\text{P}_2\text{O}_5-50\text{SiO}_2$ (in mol%) was melted from reagents: NaH_2PO_3 ($\geq 99.5\%$ SIGMA ALDRICH), Na_2CO_3 (99.9 + % ChemPur GmbH), CaCO_3 (99.9 + % ChemPur GmbH) and SiO_2 (99.99% ChemPur GmbH). Alumina crucibles were used for melting at temperatures of 1350 °C, under air atmosphere. The melts were quenched in water.

Two glass series were synthesized upon re-melting with metallic Ca or Mg. The first series had the target batch composition $x\text{Mg}-(100-x)(25\text{Na}_2\text{O}-20\text{CaO}-5\text{P}_2\text{O}_5-50\text{SiO}_2)$ (in mol%), where $x = 1, 2, 3, 4$ and 5. In the second system, Mg (99.8% ABCR GmbH&Co) was replaced by Ca (99% ALDRICH). Powders were placed in niobium crucibles and heated in nitrogen atmosphere up to temperatures between 1450 and 1650 °C, depending on the composition, using an induction furnace [8]. The melting time was about 1 h. The melts were quenched by turning off the furnace at the end of the run, which takes about 1 h to reach room temperature.

Glass characterization

The glass composition was determined by energy-dispersive spectroscopy (EDS) measurements on fresh fractured samples, using a high-resolution scanning electron microscope (LYRA3, TESCAN) equipped with EDS detector (EDAX). The EDS analysis was conducted for three different areas of each sample and the mean values of results are listed in Table 1. The compositional accuracy is around $\pm 5\%$ standard deviation.

The topography of the samples was observed by optical microscopy using an Olympus LEXT OLS4000 confocal scanning laser microscope (CSLM). Color imaging was obtained under white LED light with an objective lens magnification of 100 × and optical magnification of 2160x. CSLM measurements were acquired on freshly fractured and alcohol cleaned samples.

Table 1 Glass IDs, analyzed glass composition and melting process parameters (temperature and time) for all glasses

ID	Analyzed composition (wt%)	Analyzed composition (at%)	Analyzed composition (mol%)	T _{melting} (°C)	t _{melting} (min)
Target glass: 25Na ₂ O–20CaO–5P ₂ O ₅ –50SiO ₂					
0	Na _{19.7} Ca _{12.2} P _{5.1} Si _{21.1} Al _{0.5} O _{41.4}	Na _{18.3} Ca _{6.5} P _{3.5} Si _{16.1} Al _{0.4} O _{55.2}	27.2Na ₂ O–19.3CaO–5.2P ₂ O ₅ –0.6Al ₂ O ₃ –47.8SiO ₂	1350	30
Series I samples: xMg–(100-x)(50SiO ₂ –25Na ₂ O–5P ₂ O ₅ –20CaO)					
1 Mg	Na _{18.6} Ca _{13.1} Mg _{0.6} P _{4.9} Si _{20.1} Nb _{0.4} Al _{0.3} O ₄₂	Na _{17.3} Ca ₇ Mg _{0.5} P _{3.4} Si _{15.3} Nb _{0.1} Al _{0.3} O _{56.1}	25.9Na ₂ O–21CaO–5.1P ₂ O ₅ –1.5MgO–0.1Nb ₂ O ₅ –0.4Al ₂ O ₃ –45.9SiO ₂	1500	60
2 Mg	Na _{18.5} Ca _{13.1} Mg _{0.8} P _{3.6} Si _{21.5} Nb _{0.5} Al _{0.3} O _{42.3}	Na _{17.2} Ca _{6.7} Mg _{0.7} P _{2.5} Si _{16.3} Nb _{0.1} Al _{0.2} O _{56.4}	25.5Na ₂ O–19.9CaO–3.7P ₂ O ₅ –2.1MgO–0.1Nb ₂ O ₅ –0.3Al ₂ O ₃ –48.4SiO ₂	1500	60
3 Mg	Na _{18.4} Ca ₁₃ Mg _{0.9} P _{3.7} Si _{21.7} Nb _{0.6} Al _{0.4} O _{41.59}	Na _{17.2} Ca _{6.9} Mg _{0.8} P _{2.5} Si _{16.6} Nb _{0.1} Al _{0.3} O _{55.6}	25Na ₂ O–20CaO–3.6P ₂ O ₅ –2.4MgO–0.1Nb ₂ O ₅ –0.4Al ₂ O ₃ –48.9SiO ₂	1450 1550	15 50
4 Mg	Na ₁₇ Ca _{12.4} Mg ₁ P _{4.2} Si _{21.6} Nb _{0.7} Al _{0.4} O _{42.7}	Na _{15.8} Ca _{6.6} Mg _{0.9} P _{2.9} Si _{16.4} Nb _{0.2} Al _{0.4} O _{56.9}	23.5Na ₂ O–19.7CaO–4.3P ₂ O ₅ –2.7MgO–0.3Nb ₂ O ₅ –0.6Al ₂ O ₃ –48.9SiO ₂	1350 1550	15 50
5 Mg	Na _{17.3} Ca _{12.6} Mg _{1.4} P _{4.5} Si _{20.2} Nb _{1.3} Al _{0.6} O _{42.2}	Na _{16.1} Ca _{6.8} Mg _{1.2} P _{3.1} Si _{15.5} Nb _{0.3} Al _{0.5} O _{56.73}	24Na ₂ O–20.3CaO–4.6P ₂ O ₅ –3.6MgO–0.4Nb ₂ O ₅ –0.7Al ₂ O ₃ –46.3SiO ₂	1300 1550	15 60
Series II samples: xCa–(100-x)(50SiO ₂ –25Na ₂ O–5P ₂ O ₅ –20CaO)					
1Ca	Na _{20.1} Ca _{11.4} P _{3.5} Si _{21.6} Nb _{0.5} Al _{0.3} O _{42.3}	Na _{18.6} Ca ₆ P _{2.4} Si _{16.3} Nb _{0.1} Al _{0.2} O _{56.1}	28.2Na ₂ O–18.2CaO–3.6P ₂ O ₅ –0.1Nb ₂ O ₅ –0.3Al ₂ O ₃ –49.5SiO ₂	1600	60
2Ca	Na _{18.8} Ca _{12.7} P _{3.9} Si ₂₂ Nb _{0.3} Al _{0.2} O ₄₂	Na _{17.4} Ca _{6.8} P _{2.7} Si _{16.7} Nb _{0.1} Al _{0.2} O ₅₆	25.8Na ₂ O–20.2CaO–4P ₂ O ₅ –0.1Nb ₂ O ₅ –0.3Al ₂ O ₃ –49.6SiO ₂	1650	60
3Ca	Na _{19.1} Ca _{13.4} P _{4.2} Si _{21.1} Nb _{0.4} Al _{0.2} O _{41.8}	Na _{17.8} Ca _{7.2} P _{2.9} Si _{16.1} Nb _{0.1} Al _{0.2} O _{55.7}	26.3Na ₂ O–21.3CaO–4.3P ₂ O ₅ –0.1Nb ₂ O ₅ –0.3Al ₂ O ₃ –47.6SiO ₂	1650	60
4Ca	Na ₁₈ Ca _{13.8} P _{4.5} Si _{21.3} Nb _{0.3} Al _{0.2} O _{41.8}	Na _{16.8} Ca _{7.4} P _{3.1} Si _{16.3} Nb _{0.1} Al _{0.2} O _{56.1}	24.9Na ₂ O–21.9CaO–4.6P ₂ O ₅ –0.1Nb ₂ O ₅ –0.3Al ₂ O ₃ –48.2SiO ₂	1600	60
5Ca	Na _{17.6} Ca _{14.3} P _{4.5} Si ₂₁ Nb _{0.4} Al _{0.3} O _{41.86}	Na _{16.5} Ca _{7.7} P _{3.2} Si _{16.1} Nb _{0.1} Al _{0.2} O _{56.1}	24.4Na ₂ O–22.8CaO–4.7P ₂ O ₅ –0.1Nb ₂ O ₅ –0.3Al ₂ O ₃ –47.6SiO ₂	1600	60

Powder X-ray diffraction (XRD) technique was used to check the amorphous nature of each sample. XRD data were collected on a PANalytical PRO MPD

instrument with Bragg–Brentano geometry with CuK_{α1} radiation over a 2θ range of 10°–70° at a step size of 0.013° and step time 53 s. The XRD

measurements were taken at room temperature on powdered samples.

Infrared spectroscopy measurements were taken with a Frontier FTIR spectrometer (PerkinElmer). Plane-parallel KBr pellets, with a thickness of 0.2 to 0.7 mm, were used. They were prepared by milling and pressing mixed powders of glass and KBr. The spectra were obtained in the absorbance mode in the range of 400–4000 cm^{-1} with a resolution of 4 cm^{-1} . Sixty-four scans were collected, and the average was used for the evaluation. The absorbance values range between 5 and 75%. Therefore, we do not expect to have reached saturation levels. For better qualitative comparison, the displayed spectra are scaled to their maximum distance (minimum to maximum) in the mid-infrared region and background corrected. The estimated error in infrared band position is $\pm 2 \text{ cm}^{-1}$.

The glass transition temperatures and temperatures of crystallization processes for each samples were measured using differential thermal analysis (DTA). Measurements were taken on powdered samples placed in Al_2O_3 crucibles, up to 1000 °C in flowing nitrogen with a NETZSCH STA 409PC instrument and a heating rate of 20 °C min^{-1} . The onset of an endothermic drift on the DTA curve was taken as representing T_g . The exothermic processes observed in all samples are correlated with crystallization processes. The thermal properties parameters were estimated with respective commercial instrumental software NETZSCH–proteus analysis. The precision in their definition depends on the selected to calculations temperature ranges and varies up to $\pm 2\%$ of determined value.

The biosolubility properties were evaluated by immersing the samples for 8 days in 5 mL of phosphate buffered saline solution (PBS) at 37 °C. The PBS solution contains 11.9 mM phosphates, 137 mM sodium chloride and 2.7 mM potassium chloride and was dissolved in proportion 1:10 in deionized water to obtain pH 7.4. Glass samples having weight ~ 0.04 – 0.09 g were used for the *in vitro* testing. After immersion, the samples were cleaned with deionized water and dried in a desiccator for 24 h at room temperature. The samples were weighed again after the immersion and the top layer of samples was examined by confocal microscope and SEM. The composition of the glass surface was determined by EDS analysis.

Results and discussion

Glass formation

Two series of Na–Ca–P–Si–O glasses doped with different content of metallic Mg or Ca were synthesized. During heating, a strong exothermic reaction (described in [21, 22]) was observed, especially in melts containing ≥ 3 mol% of Mg. These samples were re-melted a second time. Table 1 presents samples IDs, analyzed compositions and melting process parameters. The temperature at which a melt formed was found to be higher for Ca containing glasses as compared to the Mg glasses. SEM–EDS analysis shows that samples contain trace amounts of Al (0.2–0.5 at%), which originates from the ceramic crucibles of the initial melt. Additionally, niobium was found to dissolve from Nb-crucibles. In our previous paper [5], we have shown that phosphate glasses can dissolve Nb from crucible material during melting while no Nb was found in silicate glasses [7, 8]. The results showed that addition of even a small amount of P (less than 3 at%) affects the chemical stability of silicate glass so that it can dissolve Nb. The Mg and Ca content increases in series Mg and Ca glasses, respectively, as was expected.

Typical CSLM images for fractured samples: 5 Mg and 5Ca are displayed in Fig. 1a and b, respectively. There is no significant difference between series Mg and Ca samples containing different Mg and Ca content. All samples are grayish, shiny and partially transparent, whereas target glass 0 prepared in air is fully transparent. The transparency and color of the samples do not change with their composition. The dark color observed for series Mg and Ca glasses may have different origins: (1) non-oxidized metallic powder residues, (2) dissolved reduced Nb ions species (even ppm content of reduced Nb^{4+} and Nb^{3+} can give color) or (3) reduced phosphate. (Since melting was done under reducing conditions Mg/Ca and no oxygen, then it is possible to obtain P in glass). In the compositions of our samples, the analyzed O content is as expected, therefore situations (1) and (3) are the most probable.

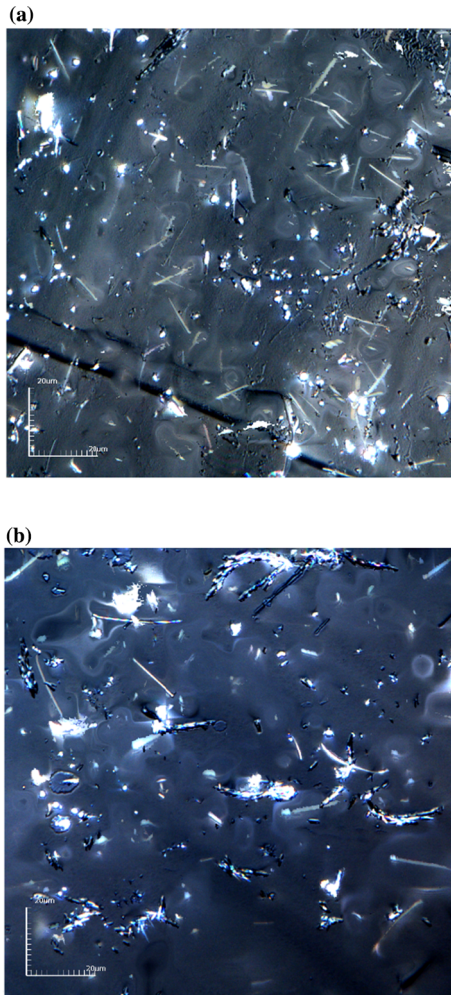


Figure 1 CSLM micrographs for fractured samples: **a** 5 Mg and **b** 5Ca scale bar shows 20 μm .

Glass structure

XRD

The amorphous nature of samples was examined by XRD measurements. Figure 2 displays the XRD curves for samples: 0, 5 Mg and 5Ca. They exhibit an amorphous halo typical for glasses. The other—not presented—samples show similar XRD curves to those depicted in Fig. 2.

Calculations of network connectivity

Before starting the spectral interpretation, let us consider how modifier oxides usually modify the glass network, and what role aluminum, magnesium and niobium ions take in various silicate glasses. Al_2O_3 is known as intermediate glass forming oxide,

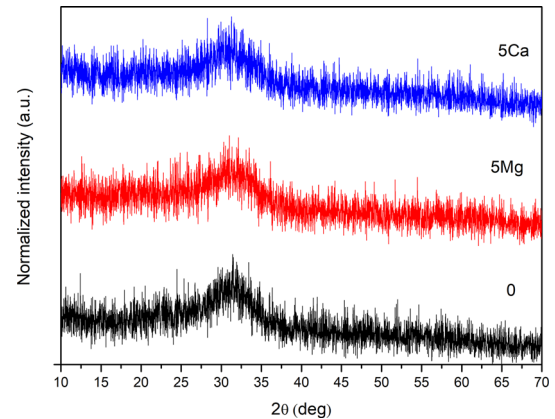


Figure 2 XRD curves for samples: 0, 5 Mg and 5Ca. Curves have been offset by maximum value to allow comparison (IDs refer to labels in Table 1).

which can act either as modifier with Al^{3+} in sixfold coordination, or as glass former with Al^{3+} in fourfold coordination, depending on alkali content [23–25]. Unexceptionally, in the case of MgO the situation can be similar to Al_2O_3 . It was shown in reference [16] that magnesium oxide is a network intermediate oxide and that charged MgO_4 tetrahedra can enter the silicate network ($\approx 14\%$ in the bioactive phosphorous–silicate glasses). However, MgO only takes the role as an intermediate oxide instead of a conventional network modifier, in highly disrupted silicate glasses, of which bioactive glasses are an example. Nb_2O_5 is a typical intermediate oxide. Raman studies of a di-silicate glass system [26] and the ^{29}Si MAS NMR studies of 45S5 bioglass doped with Nb [27] showed that Nb^{5+} ions cross-link several oxygen sites, breaking Si–O–Si bonds to form various polyhedral $[\text{Nb}(\text{OM})_6\text{y}(\text{OSi})_y]$, where $1 \leq y \leq 5$ and $\text{M}=\text{Na}, \text{Ca}$ or P . For the P-containing bioglass, Nb–O–P bonds are only present in the terminal sites. Additionally, it has to be mentioned that phosphorus in phosphorous–silicate glasses exists generally as an orthophosphate complex, rather than entering the silicate glass network. It means that P_2O_5 forms $[\text{PO}_4]^{3-}$ tetrahedra first, and only the remaining O atoms modify the silicate network [28, 29].

Table 2 presents the values of O:Si ratio calculated for the case of phosphorus in orthophosphate environment as mentioned above. The other oxides (MgO , CaO , Nb_2O_5 , Na_2O and Al_2O_3) were assumed to act as modifiers to facilitate calculations, since their role in glass network may change. The values of O:Si ratio vary between 2.56 and 2.85 and indicate silicate

network with half of Q^2 (silicon tetrahedra with two bridging oxygens–2 bO) and half of Q^3 (3 bO) units.

The other parameter, which can help during the structure results interpretation, is network connectivity (NC) of glass, defined as the average number of bonds that link each repeat unit in the network. The calculation of network connectivity of a glass is based on the relative number of network-forming oxide species (those which contribute bO species) and network modifying species (those which result in the formation of nbOs) present [33]. By comparing the NC of glass compositions with different bioactivities (measured either as the rate of formation of the hydroxyapatite (HA) layer or as the bone bonding ability), an empirical upper limit around $NC = 3$ was proposed, separating bioactive ($NC < 3$) from bioinactive ($NC > 3$) glasses [34]. The qualitative interpretation of this threshold is based on the correlation between solubility and NC; low NCs denote open and fragmented glass structures, whose rapid partial dissolution in an aqueous physiological environment will lead to HA formation and bone bonding in a shorter time, compared with glasses with a more interconnected network. As a reference, the NC for the 45S5 composition would be 1.9 [31, 35]. However, as was mentioned before, the phosphorus in phospho-silicate glasses most probably exist as an orthophosphate complex ($[PO_4]^{3-}$ tetrahedra) [31, 32] and in this case the network connectivity (NC' in

Table 2) should be calculated with the use of equation [32]:

$$NC'_{Si(P)} = \frac{4[SiO_2] + 6[P_2O_5] - 2([M_2O] + [M'O])}{[SiO_2]} \quad (1)$$

In that situation, the NC' for well-known 45S5 bioglass is equal 2.11 and for S53P4 is 2.54 [29] and the requirement for bioactive glass is found to be $NC' < 2.7$ [30] which is fulfilled by our glasses. Therefore, our glasses are potentially bioactive. It is worth to notice that series Mg and Ca glasses show lower values of NC' than the target glass 0 what suggests higher bioactivity.

The other parameter, effective cationic field strength (ECFS) of the modifiers in glass may help to explain behavior of different glass properties [31, 32]. For example, for glasses containing mixed modifier cations with the same valence, properties such as compactness, Young's modulus, microhardness, glass transition temperature and softening point, all increased linearly with increasing effective cationic field strength (ECFS) of the modifiers, whereas the MV and the thermal expansion coefficient decreased [32]. However, in our previous paper [31] we showed that in mixed modifier systems in which cation valences are not equal, such as Na–Ca–(La)–Si–O glasses, ECFS correlations may be also required to explain property variations such as glass transition temperature and glass thermal stability. Effective cationic field strengths of the compositions (see Tab. 2) were calculated using the expression:

$$ECFS = CFS_{M1} \cdot \frac{C_{M1}}{C_{M1} + C_{M2} + C_{M3} + C_{M4} + C_{M5}} + CFS_{M2} \cdot \frac{C_{M2}}{C_{M1} + C_{M2} + C_{M3} + C_{M4} + C_{M5}} + CFS_{M3} \cdot \frac{C_{M3}}{C_{M1} + C_{M2} + C_{M3} + C_{M4} + C_{M5}} + CFS_{M4} \cdot \frac{C_{M4}}{C_{M1} + C_{M2} + C_{M3} + C_{M4} + C_{M5}} + CFS_{M5} \cdot \frac{C_{M5}}{C_{M1} + C_{M2} + C_{M3} + C_{M4} + C_{M5}} \quad (2)$$

where CFS_{M1} , CFS_{M2} , CFS_{M3} , CFS_{M4} and CFS_{M5} are the cationic field strengths of the M_1 , M_2 , M_3 , M_4 and M_5 cations, and C_{M1} , C_{M2} , C_{M3} , C_{M4} and C_{M5} are their respective concentrations in atomic percent. The cation field strengths (CFS) of the modifier ions were calculated using $CFS = Z/r^2$ where "Z" is the valence of the respective cation and "r" the Shannon–Prewitt

Table 2 O:Si ratio assumes that P_2O_5 forms $[PO_4]^{3-}$ tetrahedra first, and only the remaining O atoms modify the silicate network, NC' also takes account of phosphorus in orthophosphate environment (Eq. 1). Table 2 contains also ECFS values (calculated according to Eq. 2) for all glasses

ID	O:Si	NC'	ECFS (\AA^{-2})
0	2.56	2.68	1.085
1 Mg	2.78	2.53	1.175
2 Mg	2.85	2.48	1.169
3 Mg	2.74	2.46	1.207
4 Mg	2.77	2.62	1.291
5 Mg	2.87	2.48	1.368
1Ca	2.84	2.55	1.051
2Ca	2.71	2.61	1.091
3Ca	2.73	2.52	1.096
4Ca	2.68	2.61	1.117
5Ca	2.70	2.60	1.130

ionic radius for eight-coordinated Na, seven-coordinated Ca, six-coordinated Mg, Al and Nb which is 0.718, 1.780, 3.856, 6.584, 8.218 Å⁻² for Na⁺, Ca²⁺, Mg²⁺, Al³⁺, Nb⁵⁺, respectively. The results of ECFS are discussed in **Thermal properties** Section while describing the thermal properties of glasses.

FTIR

The FTIR spectra for all series Mg and Ca glasses are shown in Fig. 3a and b, respectively. The FTIR spectrum of the target 27.2Na₂O–19.3CaO–5.2P₂O₅–0.6Al₂O₃–47.8SiO₂ (in mol%) glass exhibits the strongest IR bands (glass 0 in Figs. 3) at 932 and 1039 cm⁻¹, while another two weaker bands are seen around 486 and 757 cm⁻¹. According to the literature [10–12, 33], the strongest high-frequency bands have been assigned to Si–O band vibration (Q²) and Si–O–Si stretch band, respectively. However, band at 1030 cm⁻¹ may be also assigned to $\nu_{as}(\text{PO}_4^{3-})$ (Q⁰) [34, 35]. The band at ca. 486 and 757 cm⁻¹ are due to bending modes of Si–O–Si or O–Si–O and Si–O–Si symmetric stretching vibrations of bridging oxygens between two adjacent SiO₄ tetrahedra, respectively. Additionally, parent glass 0 shows a characteristic band envelop at ~ 575 cm⁻¹ with a pronounced splitting at ~ 598 cm⁻¹ [36] which is typical for nanometer size crystallites consisted of apatitic PO₄³⁻ groups [11, 12, 37]. This composition has NC' of 2.68 (see Table 2), which suggests highly disrupted silicate network. Its O:Si ratio is equal 2.56 that indicates primarily Q³ and some Q² silicate units. This result is underestimated since IR spectrum result suggests domination of Q² units (for which O:Si ratio should be ~ 2.8–2.9) (Fig. 3) and the difference can be due to our assumption on the role of other modifying oxides (Al₂O₃, Nb₂O₅ and MgO).

All series Mg and Ca glasses also present similar IR bands to the parent glass 0. However, these glasses show only a small single band ~ 568–591 cm⁻¹ what indicates the presence of non-apatitic or amorphous calcium phosphate (ACP). Usually, ACP indicates the presence of precursors to apatite in material [38]. The intensity of this band decreases with increase in xMg or xCa content in both glass series. These changes may suggest that the content of ACP is lower in modified glasses than in glass 0. Moreover, we note that the weak IR band at 757 cm⁻¹, connected to Si–O–Si symmetric stretching vibrations of bridging oxygens between two adjacent SiO₄ tetrahedra,

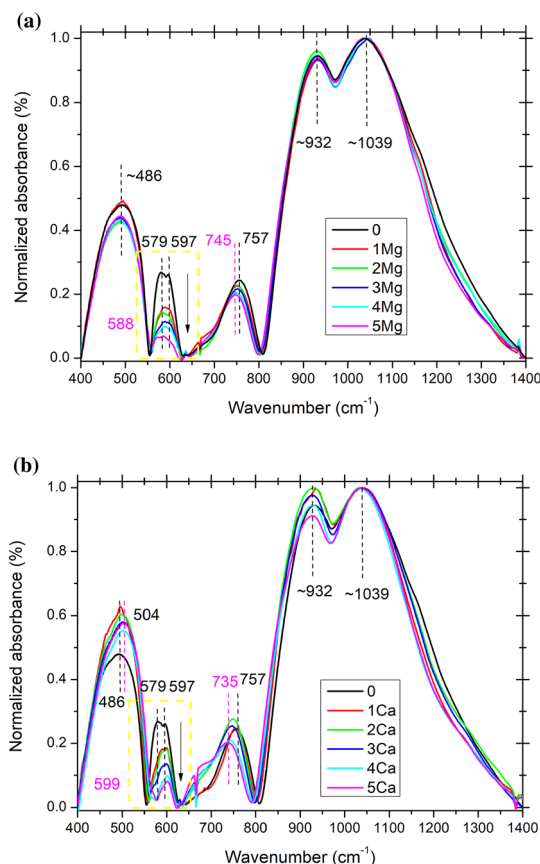


Figure 3 FTIR spectra for series **a** Mg and **b** Ca glasses. Bands positions are indicated for samples in each figure. Spectra have been normalized to the maximum value to allow comparison.

moves to lower energies for glasses xMg and xCa and decreases with increase in Mg or Ca level to ~ 745 or 735 cm⁻¹ for glasses 5 Mg and 5Ca, respectively (presented in Figs. 3).

Thermal properties

The DTA results obtained for all samples have similar characteristics. The DTA curves of all materials show a glass transition temperature and two exothermic processes. The parent glass 0 shows T_g of value of 537 °C. For the phosphate and borate glasses, if high field strength Mg²⁺ ions replace low field strength ions like Ca²⁺ or Na⁺, the T_g increases, just as addition of Al₂O₃ depolymerizes the phosphate network but increases the T_g by strong P–O–Al cross-links [39, 40]. The silicate glasses show the opposite trend than borate or phosphate glasses for alkali ions, though were supposed to give the same trend for alkaline earth ions [29, 41]. To take into account also the Al and Nb amounts leached into the glass from

the alumina and niobium crucibles, in Fig. 4a the glass transition temperature is depicted as a function of the Mg/Ca + Al + Nb content for both glass systems. Almost all modified glasses show a slightly higher T_g than the parent glass 0. An approximately linear increase of T_g with Mg + Al + Nb level is demonstrated for series xMg while series xCa glasses exhibit higher values of T_g than the ones of xMg series—this trend is unexpected for silicate glasses [29, 41]. The possible explanation is that the combined MO + Al₂O₃ + Nb₂O₅ content modifies the Mg series more than the Ca series, such decreasing the T_g .

Additionally, the T_g variations as a function of ECFS for both glass series are shown in Fig. 4b. ECFS was calculated so as to take into account all modifier ions: Na⁺, Ca²⁺, Mg²⁺, Al³⁺, Nb⁵⁺. As expected within each series, the changes in ECFS follow the changes in x. An approximately linear increase of T_g with ECFS is demonstrated for series xMg.

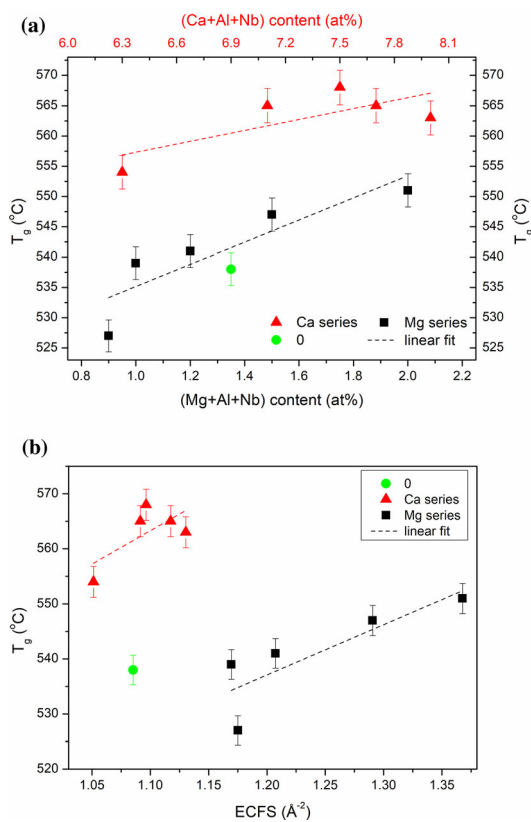


Figure 4 Comparison of glass transition temperatures as a function of **a** (Mg + Nb + Al) for series Mg glasses or (Ca + Nb + Al) content for series Ca glasses and **b** ECFS. Dashed lines show linear fit of thermal properties and are given as guide for the eyes only.

The glass stability is an often-used indicator describing the resistance to crystallization during heating. It is typically expressed by the difference between the first crystallization onset value and the glass transition temperature, the first exothermic peak position and glass transition temperature $S = T_{\text{exo1, peak}} - T_{g \text{ onset}}$ [42]. The parent glass 0 exhibits S equals 119 °C. The S values as a function of Mg/Ca + Al + Nb content are shown in Fig. 5a. S parameter mostly increases with increase in Mg/Ca + Al + Nb content for both glass series. S values vary between 160 °C observed for the glass 1 Mg and 245 °C found for the 4Ca. All glasses show higher glass stability than the parent glass 0.

The glass stability S values were additionally plotted against ECFS (see Fig. 5b). The S parameter mostly increases with increase in ECFS level for both glass series. The glass stability of well-known bioactive glasses ranges of 163 °C for 45S5 and 187 °C for S53P4 [13, 14]. Most of series Mg and Ca glasses exhibit higher S than both glasses 45S5 and S53P4 what was the aim of this work.

Biosolubility in PBS

The results of the biosolubility test in PBS are listed in Table 3. It can be seen that after 8 days of immersion in PBS, all samples show measurable loss of weight. The % change of mass varies between 0.2 and 1.1 depending on samples composition. The highest % decrease in weight was found for samples 2 Mg and 1Ca while the lowest for glasses 5 Mg and 5Ca. The potential bioactivity of glasses was investigated in terms of HAp layer formation on their surfaces after immersion in PBS. Figure 6 shows the CLSM images for surfaces of exemplary glasses (a) 0Si, (b) and (c) 2 Mg, (d) 5 Mg, (e) 2Ca and (f) 5Ca in μm scale. All the glasses have a continuous layer consisting of lobes of different sizes and shapes. The mean size of the lobes is around 100 μm . Additionally, long thin cobwebs appeared on the surface of each sample, which are visible as white luminous structures. Furthermore, glass sample 2 Mg has elongated small needles as shown in Fig. 6b–c.

Figure 7 displays SEM images of surfaces after immersion in PBS for 8 days for exemplary samples: (a) 0Si, (b) and (c) 4 Mg, (d) and (e) 2Ca, and (f) 5Ca. SEM observations showed that the glasses have thin cobwebs and granules as also observed by the confocal microscopy. Furthermore, all glasses contain

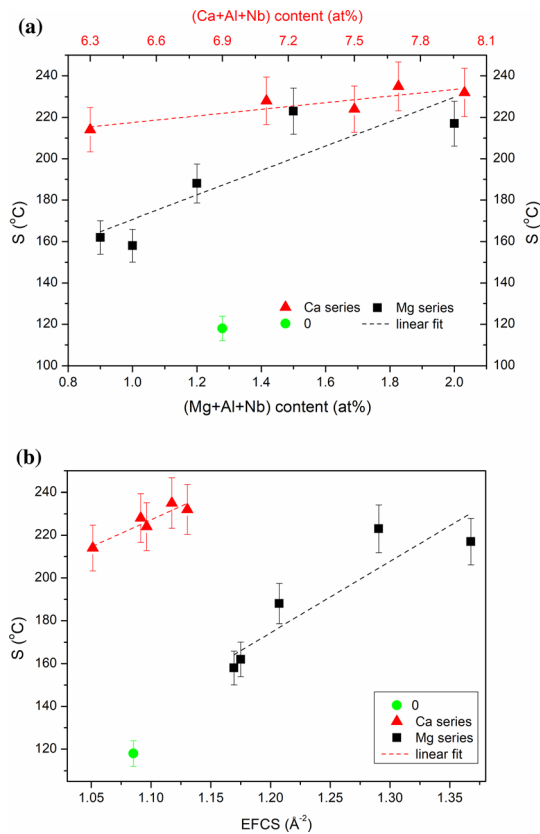


Figure 5 Comparison of glass stabilities *S* as a function of **a** (Mg + Nb + Al) for series Mg glasses or (Ca + Nb + Al) content for series Ca glasses and **b** ECFS for series *x*Mg and *x*Ca glasses. Dashed lines show trends of thermal properties and are given as guide for the eyes only.

elongated needles having sizes typically less than 2 μm. These results are in line with the SEM images of HAp layer observed for SiO₂–CaO–P₂O₅ bioactive xerogels doped with molybdenum [43]. An approximate thickness of the layer formed at surface of glass

4 Mg as a result of the biosolubility test was found to be less than 10 μm (see Fig. 7c).

To confirm the formation of HAp nucleation on the glass surface, the composition of glasses surfaces after immersion in PBS was analyzed by EDS. The EDS measurements were taken for three different areas, and the mean value of all results is presented as a representative one, see Table 3. The EDS results show that for all glasses, the contents of Ca and P on the surface significantly increased after immersion in PBS as compared with the analyzed glasses compositions obtained after the melting process (Table 1). However, the amounts of Na and Si significantly decreased in most of samples. The EDS analysis was also carried out on selected spots to compare the composition of granules and cobwebs. The results showed that they contain Ca, P and O elements having an approximate Ca/P ratio of 1.7, which is similar to the one of HAp 1.67.

The pH of PBS solutions was measured before and after the biosolubility test. It was found that the pH increased from 7.4 to approximately 8.5 after 8 days of glasses incubation. A similar increase in pH in HEPES ([4-(2-hydroxyethyl)-1-piperazineethanesulfonic acid] buffered solution) was also observed for SiO₂–Na₂O–CaO–P₂O₅–Nb₂O₅ glass system [27] having P₂O₅ content two times lower than our glasses. This increase in pH may be explained by processes occurred between the bioglass surface and body fluid: (i) rapid exchange of Na⁺/Ca²⁺ from glass network with H₃O⁺ from solution, (ii) loss of soluble silica/ formation of silanol groups at the glass solution interface, (iii) condensation and repolymerization of a SiO₂-rich layer, (iv) growth of the amorphous CaO–P₂O₅-rich film by incorporation of

Table 3 Results of biosolubility test: loss of weight and mean chemical composition of samples surfaces after 8 days of incubation in PBS

ID	Loss of weight (%)	Na (at%)	Ca (at%)	Mg (at%)	P (at%)	Si (at%)
0	0.5	4.3	12.1	–	8.7	18.2
1 Mg	0.5	5.2	21.2	1.3	16	0.2
2 Mg	1.1	0.5	29.5	0.3	13.7	–
3 Mg	0.6	3.5	21.6	1.9	16.2	0.8
4 Mg	0.6	12.2	9.5	1.5	10.3	8.7
5 Mg	0.2	4.3	10.8	2.6	10.2	14.4
1Ca	1.0	6.4	18.8	–	12.4	4.1
2Ca	0.6	4.3	23.0	–	16.4	1.0
3Ca	0.6	2.8	24.1	–	15.8	0.3
4Ca	0.6	5.4	13.9	–	10.5	12.4
5Ca	0.3	5.2	20.5	–	14.7	2

Figure 6 Confocal microscope images after immersion in PBS for 8 days for glasses: **a** 0Si, **b** and **c** 2 Mg, **d** 5 Mg, **e** 2Ca and **f** 5Ca in μm scale.

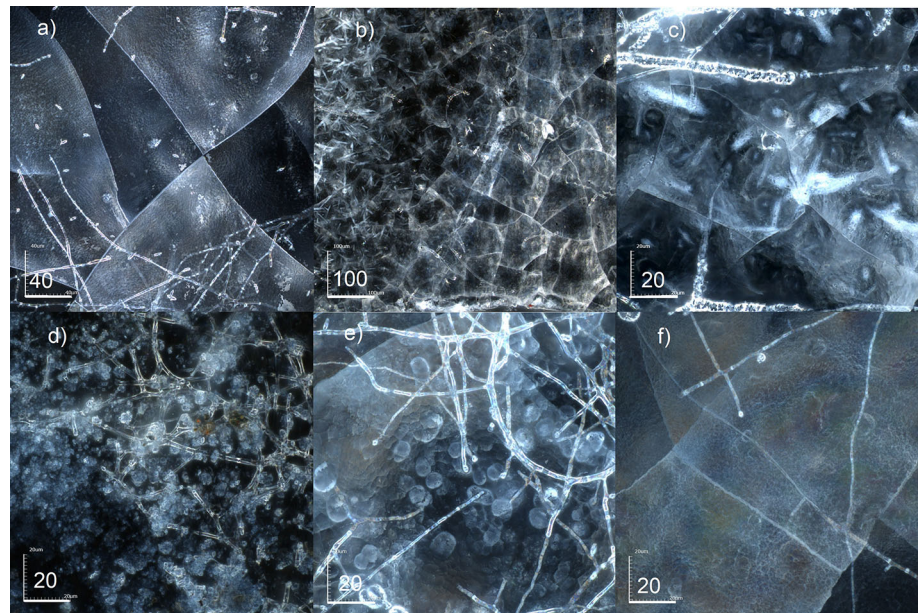
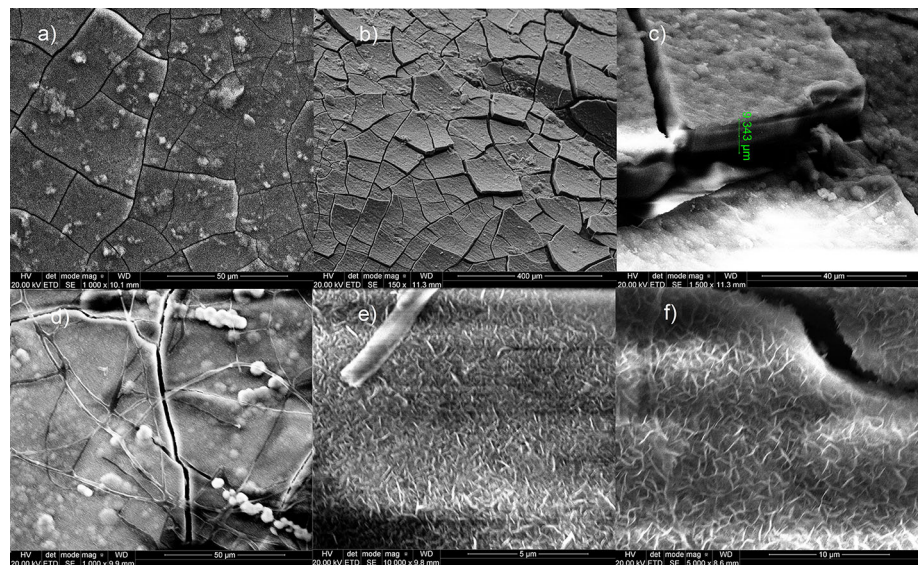


Figure 7 SEM images of surfaces after immersion in PBS for 8 days for glasses: **a** 0Si, **b** and **c** 4 Mg, **d** and **e** 2Ca and **f** 5Ca. In Fig 7c the approximate thickness of the layer formed at surface of glass 4 Mg as a result of the biosolubility test is written in green color.



soluble calcium and phosphates from solution and (v) crystallization of the amorphous $\text{CaO-P}_2\text{O}_5$ film by incorporation of OH^- and CO_3 , described in [44–46]. This mechanism of HAp layer formation was also observed in $\text{SiO}_2\text{-Na}_2\text{O-CaO-P}_2\text{O}_5\text{-Nb}_2\text{O}_5$ glasses with a significantly lower amount of P_2O_5 and higher content of Nb_2O_5 [47]. Moreover, the ion dissolution studies of these glasses [47] showed that at the beginning of immersion, the highest content of Na^+ is leached from the glass surface into the HEPES solution. Also, a high amount of Ca^{2+} dissolved into the HEPES while only a slight amount of Si ions got into the solution during the biosolubility test

regardless of the doping with Nb [47]. Based on the EDS results, we may suspect that in the case of our glasses also a high amount of sodium ions leached from the glass surface into the PBS solution. However, the observed significantly higher amount of Ca ions on the glasses surfaces indicates that after 8 days of immersion they are adsorbed on the surface from the PBS. As we can clearly see in the layer of HAp, most probably after 8 days of the PBS test, all five processes [44–46] have already passed.

Samples 4 Mg and 5 Mg which contain the highest amount of Nb and Mg exhibit the lowest increase in Ca content and high content of Si on their surfaces.

The highest chemical durability of sample 5 Mg in PBS is in agreement with the findings that Nb-rich bioglass compositions showed increased glass durability, most likely due to the formation of strong Nb–O–Si bonds [27]. Generally, the addition of Mg to bioglass adversely affects the formation rate of the HAp layer [48] but glass 2 Mg showed the fastest biosolubility in the PBS and contains only Ca and P elements on its surface. Glasses xMg and xCa mostly exhibit lower chemical durability in PBS than target glass 0, which might be due to the different melting processes. All these results reveal the potential bioactive character of tested glasses doped with Mg, Ca and Nb metals and melted under the reducing atmosphere.

Conclusions

In summary, we have prepared potential bioactive niobium doped Na–Ca–(Mg)–P–Si–O glasses using untypical two-step synthesis route and reducing atmosphere. All obtained glasses are X-ray amorphous. The color and transparency of the parent glass are affected by the addition of Ca/Mg metal and reducing atmosphere during melting process. Niobium incorporation was confirmed by SEM–EDS. The network connectivity of modified glasses is slightly lower than the one of the parent glasses and suggests bioactive properties. Network connectivity values are in agreement with FTIR spectra results, which indicate a highly disrupted silicate network, consisting mostly of Q^2 groups. FTIR spectra indicate the presence of orthophosphate complex ($[PO_4]^{3-}$ tetrahedra) in all glasses. Moreover, it is shown that parent glass contains nanometer size crystallites consisted of apatitic PO_4^{3-} groups, and the modified glasses contain non-apatitic or amorphous calcium phosphates. Thermal properties analysis shows that modified glasses exhibit a higher glass transition temperature and thermal glass stability values. Glasses doped with Ca show higher improvement in thermal properties than the one observed for glasses with Mg, which is due to the combined $MO + Al_2O_3 + Nb_2O_5$ content influence. The biosolubility test in the PBS showed that all prepared glasses exhibit potential bioactive character and the formation of HAp layer occurred on their surfaces. Furthermore, the addition of niobium slightly reduces the biosolubility of these glasses.

Acknowledgements

We want to thank Mirva Ericsson for XRD measurements and Ehsan Ghassemali for SEM–EDS measurements. We want to thank Doris Möncke for helpful discussions.

Author contributions

NAW contributed to investigation, validation, investigation, writing—original draft and visualization; SA helped in methodology, contributed to supervision, writing—review and editing, and visualization; AMG helped in PBS test; BJ helped in methodology, contributed to supervision, writing—review and editing.

Data availability

The data that support the findings of this study are available from the corresponding author upon reasonable request.

Compliance with ethical standards

Conflict of interest The authors wish to confirm that there are no known conflicts of interest associated with this publication and there has been no significant financial support for this work that could have influenced its outcome. J Mater Sci manuscript has been read and approved by all named authors.

Open Access This article is licensed under a Creative Commons Attribution 4.0 International License, which permits use, sharing, adaptation, distribution and reproduction in any medium or format, as long as you give appropriate credit to the original author(s) and the source, provide a link to the Creative Commons licence, and indicate if changes were made. The images or other third party material in this article are included in the article's Creative Commons licence, unless indicated otherwise in a credit line to the material. If material is not included in the article's Creative Commons licence and your intended use is not permitted by statutory regulation or exceeds the permitted use, you will need to obtain permission directly from the copyright holder. To view a copy of this licence, visit <http://creativecommons.org/licenses/by/4.0/>.

References

- [1] Jones JR (2013) Review of bioactive glass: from Hench to hybrids. *Acta Biomater* 9(1):4457–4486
- [2] Kokubo T (1991) Bioactive glass-ceramics-properties and applications. *Biomater* 12(2):155–163
- [3] LeGeros RZ (2002) Properties of osteoconductive biomaterials: Calcium phosphates. *Clin Orthop Relat R* 395:81–98
- [4] Bachar A, Mercier C, Tricoteaux A, Leriche A, Follet C, Hampshire S (2016) Bioactive oxynitride glasses: synthesis, structure and properties. *J Eur Ceram Soc* 36(12):2869–2881
- [5] Wójcik NA, Jonson B, Möncke D, Palles D, Kamitsos EI, Ghassemali E, Seifeddine S, Eriksson M, Ali S (2018) Influence of synthesis conditions on glass formation, structure and thermal properties in the $\text{Na}_2\text{O}-\text{CaO}-\text{P}_2\text{O}_5$ system doped with Si_3N_4 and Mg. *J Non-Cryst Solids*. <https://doi.org/10.1016/j.jnoncrystol.2018.04.055>
- [6] Ali S, Jonson B (2011) Compositional effects on the properties of high nitrogen content alkaline-earth silicon oxynitride glasses, $\text{AE}=\text{Mg, Ca, Sr, Ba}$. *J Eur Ceram Soc* 31(4):611–618
- [7] Sharafat A, Grins J, Esmailzadeh S (2008) Glass-forming region in the $\text{Ca}-\text{Si}-\text{O}-\text{N}$ system using CaH_2 as Ca source. *J Eur Ceram Soc* 28(14):2659–2664
- [8] Ali S, Jonson B, Rouxel T (2011) Glasses in the $\text{Ba}-\text{Si}-\text{O}-\text{N}$ system. *J Am Ceram Soc* 94(9):2912–2917
- [9] Sharafat A, Grins J, Esmailzadeh S (2009) Properties of high nitrogen content mixed alkali earth oxynitride glasses (AExCa_{1-x}) $_{1.2}$ (1)SiO $_{1.9}$ (1)N $_0$. 86(6), $\text{AE}=\text{Mg, Sr, Ba}$. *J Non-Cryst Solid* 355(22–23):1259–1263
- [10] Bachar A, Mercier C, Tricoteaux A, Leriche A, Follet C, Saadi M, Hampshire S (2012) Effects of addition of nitrogen on bioglass properties and structure. *J Non-Cryst Solids* 358(3):693–701
- [11] Mneimne M, Hill RG, Bushby AJ, Brauer DS (2011) High phosphate content significantly increases apatite formation of fluoride-containing bioactive glasses. *Acta Biomater* 7(4):1827–1834
- [12] O'Donnell MD, Watts SJ, Hill RG, Law RV (2009) The effect of phosphate content on the bioactivity of soda-lime-phosphosilicate glasses. *J Mater Sci-Mater M* 20(8):1611–1618. <https://doi.org/10.1007/s10856-009-3732-2>
- [13] Massera J, Fagerlund S, Hupa L, Hupa M (2012) Crystallization mechanism of the bioactive glasses, 45S5 and S53P4. *J Am Ceram Soc* 95(2):607–613
- [14] Fagerlund S, Hupa L (2016) Melt-derived bioactive silicate glasses. In: *Bioactive glasses*. <https://doi.org/10.1039/9781782622017-00001>
- [15] Vallet-Regi M, Salinas AJ, Roman J, Gil M (1999) Effect of magnesium content on the in vitro bioactivity of $\text{CaO}-\text{MgO}-\text{SiO}_2-\text{P}_2\text{O}_5$ sol-gel glasses. *J Mater Chem* 9(2):515–518
- [16] Watts SJ, Hill RG, O'Donnell MD, Law RV (2010) Influence of magnesia on the structure and properties of bioactive glasses. *J Non-Cryst Solids* 356(9):517–524
- [17] Yamamoto A, Honma R, Sumita M (1998) Cytotoxicity evaluation of 43 metal salts using murine fibroblasts and osteoblastic cells. *J Biomed Mater Res* 39(2):331–340
- [18] Obata A, Takahashi Y, Miyajima T, Ueda K, Narushima T, Kasuga T (2012) Effects of niobium ions released from calcium phosphate invert glasses containing Nb_2O_5 on osteoblast-like cell functions. *ACS Appl Mater Interfac* 4(10):5684–5690
- [19] de Souza LPL, Lopes JH, Ferreira FV, Martin RA, Bertran CA, Camilli JA (2020) Evaluation of effectiveness of 45S5 bioglass doped with niobium for repairing critical-sized bone defect in in vitro and in vivo models. *J Biomed Mater Res, Part A* 108(3):446–457
- [20] Miguez-Pacheco V, de Ligny D, Schmidt J, Detsch R, Boccaccini AR (2018) Development and characterization of niobium-releasing silicate bioactive glasses for tissue engineering applications. *J Eur Ceram Soc* 38(3):871–876
- [21] Ali S, Grins J, Esmailzadeh S (2008) Glass-forming region in the $\text{Ca}-\text{Si}-\text{O}-\text{N}$ system using CaH_2 as Ca source. *J Eur Ceram Soc* 28(14):2659–2664
- [22] Ali S, Grins J, Esmailzadeh S (2009) Properties of high nitrogen content mixed alkali earth oxynitride glasses (AExCa_{1-x}) $_{1.2}$ (1)SiO $_{1.9}$ (1)N $_0$. 86(6), $\text{AE}=\text{Mg, Sr, Ba}$. *J Non-Cryst Solids*. <https://doi.org/10.1016/j.jnoncrystol.2009.04.036>
- [23] Morin E, Wu J, Stebbins J (2014) Modifier cation (Ba, Ca, La, Y) field strength effects on aluminum and boron coordination in aluminoborosilicate glasses: the roles of fictive temperature and boron content. *Appl Phys A* 116(2):479–490
- [24] Le Losq C, Neuville DR, Florian P, Henderson GS, Massiot D (2014) The role of Al^{3+} on rheology and structural changes in sodium silicate and aluminosilicate glasses and melts. *Geochim Cosmochim Acta*. <https://doi.org/10.1016/j.gca.2013.11.010>
- [25] Thompson LM, Stebbins JF (2012) Non-stoichiometric non-bridging oxygens and five-coordinated aluminum in alkaline earth aluminosilicate glasses: effect of modifier cation size. *J Non-Cryst Solids* 358(15):1783–1789
- [26] Möncke D, Ehart R, Palles D, Efthimiopoulos I, Kamitsos EI, Johannes M (2017) A multi technique study of a new lithium disilicate glass-ceramic spray-coated on ZrO_2 substrate for dental restoration. *Biomed Glasses*. <https://doi.org/10.1515/bglass-2017-0004>

- [27] Lopes JH, Magalhães A, Mazali IO, Bertran CA (2014) Effect of niobium oxide on the structure and properties of melt-derived Bioactive glasses. *J Am Ceram Soc* 97(12):3843–3852
- [28] O'Donnell MD, Watts SJ, Law RV, Hill RG (2008) Effect of P₂O₅ content in two series of soda lime phosphosilicate glasses on structure and properties—Part I: NMR. *J Non-Cryst Solids* 354(30):3554–3560
- [29] Brauer DS, Moncke D (2017) Introduction to the structure of silicate, phosphate and borate glasses. In: *Bioactive glasses: fundamentals, technology and applications*. The royal society of chemistry. <https://doi.org/10.1039/9781782622017-00061>
- [30] Edén M (2011) The split network analysis for exploring composition–structure correlations in multi-component glasses: I. rationalizing bioactivity–composition trends of bioglasses. *J Non-Cryst Solids* 357(6):1595–1602
- [31] Ali S, Wójcik NA, Jonson B, Kamitsos EI, Li X, Luo J, Möncke D Synthesis, structural characterization, and thermal properties of Ca-and La-doped soda-lime glasses by laser melting. *Int J Appl Glass Sci*
- [32] Pomeroy MJ, Nestor E, Ramesh R, Hampshire S (2005) Properties and crystallization of rare-earth Si–Al–O–N glasses containing mixed trivalent modifiers. *J Am Ceram Soc* 88(4):875–881
- [33] ElBatal HA, Hassaan MY, Fanny MA, Ibrahim MM (2017) Optical and FT infrared absorption spectra of soda lime silicate glasses containing nano Fe₂O₃ and effects of gamma irradiation. *Silicon* 9(4):511–517
- [34] Moustafa YM, El-Egili K (1998) Infrared spectra of sodium phosphate glasses. *J Non-Cryst Solids* 240(1–3):144–153
- [35] Konidakis I, Varsamis CPE, Kamitsos EI, Moncke D, Ehrtd D (2010) Structure and properties of mixed strontium-manganese metaphosphate glasses. *J Phys Chem C* 114(19):9125–9138
- [36] Rey C, Combes C, Drouet C, Lebugle A, Sfihi H, Barroug A (2007) Nanocrystalline apatites in biological systems: characterisation, structure and properties. *Mater Werkst* 38(12):996–1002
- [37] Legeros RZ, Trautz OR, Klein E, Legeros JP (1969) 2 Types of carbonate substitution in apatite structure. *Exp*. <https://doi.org/10.1007/BF01903856>
- [38] Jones JR, Sepulveda P, Hench LL (2001) Dose-dependent behavior of bioactive glass dissolution. *J Biomed Mater Res* 58(6):720–726
- [39] Konidakis I, Varsamis CPE, Kamitsos EI (2011) Effect of synthesis method on the structure and properties of AgPO₃-based glasses. *J Non-Cryst Solids* 357(14):2684–2689
- [40] Palles D, Konidakis I, Varsamis CPE, Kamitsos EI (2016) Vibrational spectroscopic and bond valence study of structure and bonding in Al₂O₃-containing AgI–AgPO₃ glasses. *RSC Adv* 6(20):16697–16710
- [41] Natrup F, Bracht H (2005) Correlation between the cation radii and the glass transition in mixed cation silicate glasses. *Phys Chem Glasses –Eur J Glass Sci Technol Part B* 46:95–98
- [42] Simon V, Muresan D, Takacs A, Neumann M, Simon S (2007) Local order changes induced in calcium–sodium–phosphate glasses by transition metals. *Solid State Ionics* 178(3–4):221–225
- [43] Ponta O, Ciceo-Lucacel R, Vulpoi A, Radu T, Simon S (2014) Molybdenum effect on the structure of SiO₂–CaO–P₂O₅ bioactive xerogels and on their interface processes with simulated biofluids. *J Biomed Mater Res, Part A*. <https://doi.org/10.1002/jbm.a.34989>
- [44] Hench LL, Polak JM, Xynos ID, Buttery LDK (2000) Bioactive materials to control cell cycle. *Mater Res Innov* 3(6):313–323
- [45] Hench LL, Splinter RJ, Allen WC, Greenlee TK (1971) Bonding mechanisms at the interface of ceramic prosthetic materials. *J Biomed Mater Res* 5(6):117–141. <https://doi.org/10.1002/jbm.820050611>
- [46] Lopes J, Mazali IO, Landers R, Bertran C, Kim HE (2013) Structural investigation of the surface of bioglass 45S5 enriched with calcium ions. *J Am Ceram Soc*. <https://doi.org/10.1111/jace.12305>
- [47] Souza L, Lopes JH, Encamação D, Mazali IO, Martin RA, Camilli JA, Bertran CA (2018) Comprehensive in vitro and in vivo studies of novel melt-derived Nb-substituted 45S5 bioglass reveal its enhanced bioactive properties for bone healing. *Sci Rep*. <https://doi.org/10.1038/s41598-018-31114-0>
- [48] Pérez-Pariente J, Balas F, Vallet-Regí M (2000) Surface and chemical study of SiO₂·P₂O₅·CaO·(MgO) bioactive glasses. *Chem Mater* 12(3):750–755. <https://doi.org/10.1021/cm9911114>

Publisher's Note Springer Nature remains neutral with regard to jurisdictional claims in published maps and institutional affiliations.